SpringerBriefs in Applied Sciences and Technology

Upper Bound Limit Load Solutions for Welded Joints with Cracks

Bearbeitet von
Sergey Alexandrov

1. Auflage 2012. Taschenbuch. IX, 117 S. Paperback
ISBN 978 3 642 29233 0
Format (B x L): 15,5 x 23,5 cm
Gewicht: 207 g

Chapter 2
Plane Strain Solutions for Highly Undermatched Tensile Specimens

The specimens considered in this chapter are welded plates with the weld orientation orthogonal to the line of action of tensile forces applied. A crack is entirely located in the weld. Edge cracks are excluded from consideration. The width of the plate is denoted by $2W$, its thickness by $2B$, the thickness of the weld by $2H$, and the length of the crack by $2a$ (except the last solution of this chapter which deals with cracks of arbitrary shape in the plane of flow). Since plane strain solutions are of concern in the present chapter, integration in the thickness direction in volume and surfaces integrals involved in Eq. (1.4) is replaced with the multiplier $2B$ without any further explanation. For the same reason, the term "velocity discontinuity surface" is replaced with the term "velocity discontinuity curve (or line)". The latter refers to curves (lines) in the plane of flow. Base material is supposed to be rigid.

2.1 Center Cracked Specimen

The geometry of the specimen and the directions of the axes of Cartesian coordinates (x, y) are illustrated in Fig. 2.1. The specimen is loaded by two equal forces F whose magnitude at plastic collapse should be evaluated. A numerical slip-line solution for such specimens has been proposed in Hao et al. (1997). It is evident that Eq. (1.13) is valid for the specimen under consideration. It is possible to assume that $L \equiv H$. It is first necessary to determine the limit load for the specimen with no crack, $a = 0$. It is convenient to choose the origin of the Cartesian coordinate system at the intersection of the axes of symmetry of the specimen. Then, it is sufficient to find the solution in the domain $x \geq 0$ and $y \geq 0$. Let u_x be the velocity component in the x-direction and u_y in the y-direction. The blocks of rigid base material move with a velocity U along the y-axis in the opposite directions. The velocity boundary conditions are

S. Alexandrov, *Upper Bound Limit Load Solutions for Welded Joints with Cracks*, SpringerBriefs in Computational Mechanics, DOI: 10.1007/978-3-642-29234-7_2,

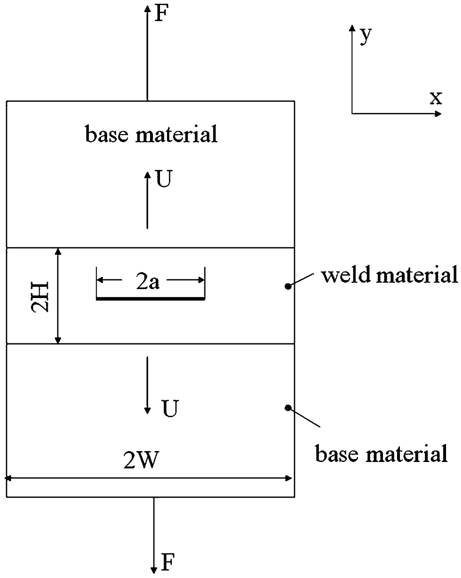

Fig. 2.1 Geometry of the specimen under consideration–notation

$$u_y = 0 \tag{2.1}$$

for $y = 0$,

$$u_x = 0 \tag{2.2}$$

for $x = 0$,

$$u_y = U \tag{2.3}$$

for $y = H$, and

$$u_x = 0 \tag{2.4}$$

for $y = H$.

The boundary conditions (2.1) to (2.4) show that the present problem is equivalent to the problem of plane strain compression of a plastic layer between two parallel, rigid plates if the maximum friction law is assumed at the surface of plates (the difference in the sense of u_y at $y = H$ is immaterial for pressure-independent materials). An approximate stress solution for the latter has been obtained by Prandtl (1923) and an approximate velocity solution by Hill (1950). Hill (1950) has also found an accurate slip-line solution. Using this solution the force can be approximated by

$$\frac{F_u^{(0)}}{4\sigma_0 BW} = \frac{1}{2\sqrt{3}}\left(3 + \frac{W}{H}\right). \tag{2.5}$$

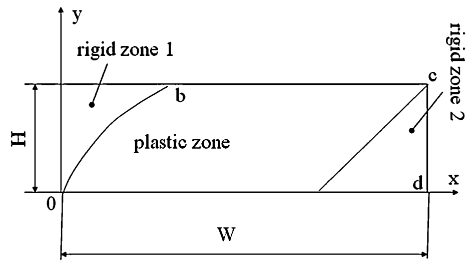

Fig. 2.2 Configuration of plastic and rigid zones from the slip-line solution

This approximation is valid for $W/H \geq 1$. A schematic diagram showing the configuration of plastic and rigid zones which follows from the slip-line solution is presented in Fig. 2.2 for one quarter of the weld. There are two velocity discontinuity curves, $0b$ and bc, and the solution satisfies Eq.(1.9) in the vicinity of line bc. It follows from Eqs. (1.10) and (2.5) that

$$\Omega(w) = \frac{(3+w)}{2\sqrt{3}}. \tag{2.6}$$

Therefore, substituting Eq. (2.6) into Eq. (1.13) gives the limit load for the cracked specimen in the form

$$f_u = \frac{F_u}{4\sigma_0 BW} = \frac{1}{2\sqrt{3}}\left(1 - \frac{a}{W}\right)\left(3 + \frac{W-a}{H}\right). \tag{2.7}$$

The restriction $W/H \geq 1$ transforms to $(W-a)/H \geq 1$. Thus the solution is not valid for large cracks. The solution for this special case is trivial and is available in the literature (see, for example, Kim and Schwalbe 2001a).

The derivation that has led to the solution (2.7) is an illustration of using Eq. (1.13) in conjunction with numerical solutions. The problem under consideration is also very suitable for illustrating the use of Eq. (1.9) in upper bound solutions. Therefore, even though it is not realistic to obtain a better result than that given by Eq. (2.7), such a solution is provided below.

A general approach to construct singular kinematically admissible velocity fields for plastic layers subject to tensile loading has been proposed in Alexandrov and Richmond (2000). The starting point of this approach is the representation of velocity components tangent to the bi-material interface in such a form that Eq. (1.9) is automatically satisfied. Then, the solution to the equation of incompressibility (1.6) gives the axial velocity in rather a complicated form. Moreover, the kinematically admissible velocity field proposed in Alexandrov and Richmond (2000) contains no rigid zone near the axis of symmetry (such as rigid zone 1 in Fig. 2.2). Therefore, a slightly different approach is developed here. It is convenient to introduce the following dimensionless quantities.

$$\frac{y}{H} = \eta, \quad \frac{x}{W} = \varsigma, \quad \frac{H}{W} = h. \tag{2.8}$$

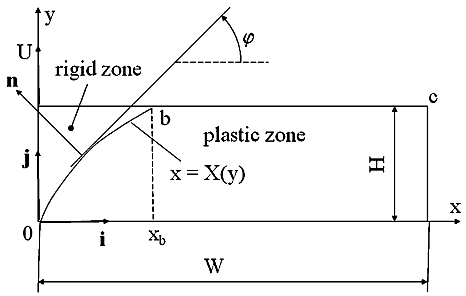

Fig. 2.3 General structure of the kinematically admissible velocity field

The starting point of the present approach is a linear through-thickness distribution of the axial velocity, which is quite reasonable because the thickness of the layer is small as compared to its width. Then, the boundary conditions (2.1) and (2.3) along with Eq. (2.8) require that

$$\frac{u_y}{U} = \eta. \tag{2.9}$$

The equation of incompressibility (1.6) in the case under consideration reduces to

$$h\frac{\partial u_x}{\partial \varsigma} + \frac{\partial u_y}{\partial \eta} = 0. \tag{2.10}$$

Substituting Eq. (2.9) into Eq. (2.10) and integrating give

$$\frac{u_x}{U} = -\frac{\varsigma}{h} + g(\eta) \tag{2.11}$$

where $g(\eta)$ is an arbitrary function of its argument. The assumption of no rigid zone and the boundary condition (2.2) require $g = 0$. However, a much better solution can be obtained without this assumption. Instead, it is assumed that there is a rigid zone near the axis $x = 0$. The general structure of the kinematically admissible velocity field in the region $0 \le x \le W$ and $0 \le y \le H$ is shown in Fig. 2.3. It is similar to that obtained from the slip-line solution (Fig. 2.2). In general, it is possible to include rigid zone 2 in consideration as well. However, a possible improvement in limit load prediction is negligible. The rigid zone (Fig. 2.3) moves in the direction of the y-axis along with the block of rigid base material. Therefore, the boundary condition (2.2) is satisfied. Also is satisfied the boundary condition (2.4) in the range $0 \le x \le x_b$. The value of x_b will be determined later. The shape of the rigid plastic boundary $0b$, which is also a velocity discontinuity curve, should be found from the solution. Let $x = X(y)$ be the equation for this curve. The velocity field is kinematically admissible if and only if this curve contains the origin of the coordinate system. Then, the following condition holds

$$X = 0 \tag{2.12}$$

for $y = 0$.

Let φ be the orientation of the tangent to the velocity discontinuity curve relative to the x-axis. Then, the unit normal vector to this curve can be represented as (Fig. 2.3)

$$\mathbf{n} = -\sin\varphi\mathbf{i} + \cos\varphi\mathbf{j} \tag{2.13}$$

where $\mathbf{i}$ and $\mathbf{j}$ are the base vectors of the Cartesian coordinate system. The velocity vector in the rigid zone is

$$\mathbf{U} = U\mathbf{j}. \tag{2.14}$$

Using Eqs. (2.9) and (2.11) the velocity field in the plastic zone can be written in the form

$$\mathbf{u} = u_x\mathbf{i} + u_y\mathbf{j} = U[-\varsigma/h + g(\eta)]\mathbf{i} + U\eta\mathbf{j}. \tag{2.15}$$

Assume that $\mathbf{U} \equiv \mathbf{u_1}$ and $\mathbf{u} \equiv \mathbf{u_2}$ in Eq. (1.7). Then, it follows from Eqs. (2.13), (2.14) and (2.15) that $[-\varsigma/h + g(\eta)]\sin\varphi + (1-\eta)\cos\varphi = 0$. Since $\tan\varphi = dy/dx$ (Fig. 2.3), this equation can be transformed, with the use of Eq. (2.8), to

$$\frac{d\varsigma}{d\eta} = \frac{\varsigma - hg(\eta)}{1-\eta}. \tag{2.16}$$

This is a linear ordinary differential equation of first order. Therefore, its general solution can be found with no difficulty. The condition (2.12) is equivalent to the condition $\varsigma = 0$ at $\eta = 0$ for Eq. (2.16). The solution to Eq. (2.16) satisfying this condition is

$$\varsigma = \varsigma_{0b}(\eta) = -\frac{h}{(1-\eta)}\int_0^\eta g(\upsilon)d\upsilon \tag{2.17}$$

where υ is a dummy variable. It is worth noting here that the denominator in Eq. (2.17) vanishes at $\eta = 1$. Therefore, the velocity discontinuity curve can have a common point with the line $\eta = 1$ (or $y = H$) if and only if the integral vanishes at $\eta = 1$. Moreover, the right hand side of Eq. (2.17) must tend to a finite limit as $\eta \to 1$. An additional condition for the validity of the subsequent solution is that the x-coordinate of point b (Fig. 2.3) should lie in the range $0 < x_b \le W$. Finally, in order to obtain the structure of the kinematically admissible velocity field shown in Fig. 2.3, it is necessary to impose the following restriction on the function $g(\eta)$

$$\varsigma_b = -h\lim_{\eta\to 1}\left[\frac{1}{(1-\eta)}\int_0^\eta g(\upsilon)d\upsilon\right] = hg(1), \quad 0 < \varsigma_b \le 1. \tag{2.18}$$

Here l'Hospital's rule has been applied and $\varsigma_b = x_b/W$.

The strain rate components and the equivalent strain rate are determined from Eqs. (1.3), (2.8), (2.9), and (2.11) as

$$\zeta_{xx} = \frac{\partial u_x}{\partial x} = -\frac{U}{H}, \quad \zeta_{yy} = \frac{\partial u_y}{\partial y} = \frac{U}{H}, \quad \zeta_{xy} = \frac{1}{2}\left(\frac{\partial u_x}{\partial y} + \frac{\partial u_y}{\partial x}\right) = \frac{Ug'(\eta)}{2H},$$
$$\zeta_{eq} = \frac{1}{\sqrt{3}}\frac{U}{H}\sqrt{4 + [g'(\eta)]^2} \tag{2.19}$$

where $g'(\eta) \equiv dg(\eta)/d\eta$. The rate of work dissipation in the plastic zone is found with the use of Eq. (2.19) in the form

$$E_V = \sigma_0 \iiint_V \zeta_{eq} dV = \frac{2UBW\sigma_0}{\sqrt{3}} \int_0^1 \int_{\varsigma_{0b}(\eta)}^1 \sqrt{4 + [g'(\eta)]^2} d\varsigma d\eta$$

or, after integration with respect to ς,

$$\frac{E_V}{4UBW\sigma_0} = \frac{1}{2\sqrt{3}} \int_0^1 [1 - \varsigma_{0b}(\eta)]\sqrt{4 + [g'(\eta)]^2} d\eta. \tag{2.20}$$

There are two velocity discontinuity curves, $0b$ and bc (Fig. 2.3). In the case of line bc, it is assumed that a material layer of infinitesimal thickness sticks at the block of rigid base material according to the boundary condition (2.4). Then, a necessity of the discontinuity follows from Eq. (2.11). Substituting Eqs. (2.14) and (2.15) into Eq. (1.8) gives the amount of velocity jump across the velocity discontinuity curve $0b$ in the form

$$|[u_\tau]|_{0b} = U\sqrt{(1-\eta)^2 + [g(\eta) - \varsigma/h]^2}. \tag{2.21}$$

Taking into account the boundary condition (2.4) the amount of velocity jump across the velocity discontinuity line bc can be represented as $|u_x|$ at $\eta = 1$ in the range $x_b \le x \le W$ (or $\varsigma_b \le \varsigma \le 1$). Therefore, it follows from Eqs. (2.11) and (2.18) that

$$|[u_\tau]|_{bc} = \frac{U}{h}(\varsigma - \varsigma_b). \tag{2.22}$$

The rate of work dissipation at the velocity discontinuity curve $0b$ is determined as

$$E_{0b} = \frac{\sigma_0}{\sqrt{3}} \iint_{S_d} |[u_\tau]|_{0b} dS = \frac{2B\sigma_0}{\sqrt{3}} \int_0^H |[u_\tau]|_{0b} \sqrt{1 + \left(\frac{dx}{dy}\right)^2} dy$$

or, with the use of Eq. (2.8),

$$E_{0b} = \frac{\sigma_0}{\sqrt{3}} \iint_{S_d} |[u_\tau]|_{0b} dS = \frac{2BH\sigma_0}{\sqrt{3}} \int_0^1 |[u_\tau]|_{0b} \sqrt{1 + \frac{1}{h^2}\left(\frac{d\varsigma}{d\eta}\right)^2} d\eta. \tag{2.23}$$

Here the derivative $d\varsigma/d\eta$ should be found at points of the velocity discontinuity curve $0b$ and is therefore given by Eq. (2.16) where ς should be replaced with $\varsigma_{0b}(\eta)$. Substituting Eqs. (2.16) and (2.21) into Eq. (2.23) leads to

$$\frac{E_{0b}}{4UBW\sigma_0} = \frac{h}{2\sqrt{3}} \int_0^1 \frac{(1-\eta)^2 + [g(\eta) - \varsigma_{0b}(\eta)/h]^2}{1-\eta} d\eta. \tag{2.24}$$

Using Eq. (2.8) the rate of work dissipation at the velocity discontinuity line bc is represented in the form

$$E_{bc} = \frac{\sigma_0}{\sqrt{3}} \iint_{S_d} |[u_\tau]|_{bc} dS = \frac{2B\sigma_0}{\sqrt{3}} \int_{x_b}^{W} |[u_\tau]|_{bc} dx = \frac{2BW\sigma_0}{\sqrt{3}} \int_{\varsigma_b}^{1} |[u_\tau]|_{bc} d\varsigma. \tag{2.25}$$

Substituting Eq. (2.22) into Eq. (2.25) and integrating lead to

$$\frac{E_{bc}}{4UBW\sigma_0} = \frac{(1-\varsigma_b)^2}{4\sqrt{3}h}. \tag{2.26}$$

The rate at which forces F do work is

$$\iint_{S_v} (t_i v_i) dS = \frac{1}{2} FU. \tag{2.27}$$

The multiplier 1/2 has appeared here because two equal forces act but one quarter of the specimen is considered. Using Eq. (2.27) the inequality (1.4) for the problem under consideration can be transformed to $F_u U = 2(E_V + E_{0b} + E_{bc})$. Substituting Eqs. (2.20), (2.24) and (2.26) into this equation gives

$$\begin{aligned} f_u &= \frac{F_u}{4BW\sigma_0} = \frac{1}{\sqrt{3}} \left[I_1 + hI_2 + \frac{(1-\varsigma_b)^2}{2h} \right], \\ I_1 &= \int_0^1 [1 - \varsigma_{0b}(\eta)] \sqrt{4 + [g'(\eta)]^2} d\eta, \\ I_2 &= \int_0^1 \frac{(1-\eta)^2 + [g(\eta) - \varsigma_{0b}(\eta)/h]^2}{1-\eta} d\eta \end{aligned} \tag{2.28}$$

It is now necessary to specify the function $g(\eta)$. It is advantageous to choose this function such that Eq. (1.9) is satisfied in the vicinity of the velocity discontinuity line bc. It is obvious from Eq. (2.19) that the normal strain rates in the Cartesian coordinate system are bounded everywhere. Therefore, it follows from Eq. (1.9) that $|\zeta_{xy}| \to \infty$ or $|\partial u_x/\partial \eta| \to \infty$ as $\eta \to 1$ in the range $\varsigma_b \le \varsigma \le 1$. Moreover, symmetry demands that $g(\eta)$ is an even function of its argument. One of the simplest functions satisfying this symmetry requirement and the inverse square root rule in Eq. (1.9) is

$$g(\eta) = \beta_0 + \beta_1\sqrt{1-\eta^2} \tag{2.29}$$

where β_0 and β_1 are free parameters. Substituting Eq. (2.29) into Eq. (2.18) shows that the limit is finite if and only if $\beta_0 = -\pi\beta_1/4$. Moreover, $\varsigma_b = -h\pi\beta_1/4$. Then, replacing β_0 and β_1 in Eq. (2.29) with ς_b and differentiating give

$$g(\eta) = \frac{\varsigma_b}{h}\left(1 - \frac{4}{\pi}\sqrt{1-\eta^2}\right), \quad g'(\eta) = \frac{4\varsigma_b}{\pi h}\frac{\eta}{\sqrt{1-\eta^2}}. \tag{2.30}$$

Substituting Eq. (2.30) into Eq. (2.17) results in

$$\varsigma_{0b}(\eta) = \frac{\varsigma_b}{\pi(1-\eta)}\left(2\eta\sqrt{1-\eta^2} + 2\arcsin\eta - \pi\eta\right). \tag{2.31}$$

In general, excluding $g(\eta)$, $g'(\eta)$ and $\varsigma_{0b}(\eta)$ on the right hand side of Eq. (2.28) the value of f_u can be evaluated using Eqs. (2.30) and (2.31). However, the integral I_1 involved in Eq. (2.28) is improper since $g'(\eta) \to \infty$ as $\eta \to 1$. Therefore, it is convenient to introduce the new variable ϑ by

$$\eta = \sin\vartheta, \quad d\eta = \cos\vartheta d\vartheta. \tag{2.32}$$

Then, using Eqs. (2.30) and (2.31) the integral I_1 can be transformed to

$$I_1 = 2\int_0^{\pi/2}\left[1 - \frac{\varsigma_b(\sin 2\vartheta + 2\vartheta - \pi\sin\vartheta)}{\pi(1-\sin\vartheta)}\right]\sqrt{\cos^2\vartheta + 4\left(\frac{\varsigma_b}{\pi h}\right)^2\sin^2\vartheta}d\vartheta. \tag{2.33}$$

A difficulty with numerical evaluating this integral is that the integrand reduces to the expression $0/0$ at $\vartheta = \pi/2$. In order to facilitate numerical integration, the integrand should be expanded in a series in the vicinity of this point. In particular,

$$\begin{aligned}&\left[1 - \frac{\varsigma_b(\sin 2\vartheta + 2\vartheta - \pi\sin\vartheta)}{\pi(1-\sin\vartheta)}\right]\sqrt{\cos^2\vartheta + 4\left(\frac{\varsigma_b}{\pi h}\right)^2\sin^2\vartheta}d\vartheta \\ &= \frac{(1-\varsigma_b)\varsigma_b}{\pi h} + \frac{8\varsigma_b^2}{3\pi^2 h}\left(\frac{\pi}{2} - \vartheta\right) + o\left(\frac{\pi}{2} - \vartheta\right), \quad \vartheta \to \frac{\pi}{2}.\end{aligned} \tag{2.34}$$

Substituting Eq. (2.34) into Eq. (2.33) and integrating analytically over the range $\pi/2 - \delta \le \vartheta \le \pi/2$ lead to

$$\begin{aligned}I_1 = &\frac{2(1-\varsigma_b)\varsigma_b}{\pi h}\delta + \frac{8\varsigma_b^2}{3\pi^2 h}\delta^2 \\ &+ 2\int_0^{\pi/2-\delta}\left[1 - \frac{\varsigma_b(\sin 2\vartheta + 2\vartheta - \pi\sin\vartheta)}{\pi(1-\sin\vartheta)}\right]\sqrt{\cos^2\vartheta + 4\left(\frac{\varsigma_b}{\pi h}\right)^2\sin^2\vartheta}d\vartheta\end{aligned} \tag{2.35}$$

where δ is a small number.

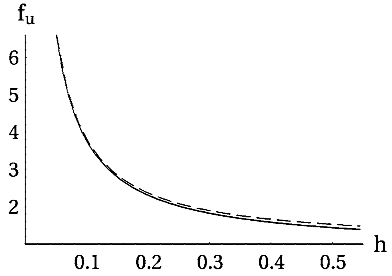

Fig. 2.4 Comparison of two solutions for the dimensionless upper bound limit load

Analogously, it is possible to verify by inspection that the integrand of the integral I_2 involved in Eq. (2.28) reduces to the expression $0/0$ at $\eta = 1$. Using Eqs. (2.30) and (2.31) to exclude $g(\eta)$ and $\varsigma_{0b}(\eta)$ this integral can be rewritten as

$$I_2 = \int_0^1 \frac{\pi^2 h^2 (1-\eta)^4 + \varsigma_b^2 \left[\begin{array}{l} \left(\pi - 4\sqrt{1-\eta^2}\right)(1-\eta) - \\ 2\eta\sqrt{1-\eta^2} - 2\arcsin\eta + \pi\eta \end{array} \right]^2}{\pi^2 h^2 (1-\eta)^3} d\eta. \qquad (2.36)$$

Expanding the integrand in a series in the vicinity of $\eta = 1$ gives

$$\frac{\pi^2 h^2 (1-\eta)^4 + \varsigma_b^2 \left[\left(\pi - 4\sqrt{1-\eta^2}\right)(1-\eta) - 2\eta\sqrt{1-\eta^2} - 2\arcsin\eta + \pi\eta\right]^2}{\pi^2 h^2 (1-\eta)^3}$$
$$= \frac{32\varsigma_b^2}{9\pi^2 h^2} + \left(\frac{16\varsigma_b^2}{5\pi^2 h^2} - 1\right)(\eta - 1) + o(\eta - 1), \quad \eta \to 1. \qquad (2.37)$$

Substituting Eq. (2.37) into Eq. (2.36) and integrating lead to

$$I_2 = \frac{1}{2} + \frac{32\varsigma_b^2}{9\pi^2 h^2}\delta - \frac{8\varsigma_b^2}{5\pi^2 h^2}\delta^2 + \frac{\varsigma_b^2}{\pi^2 h^2} \int_0^{1-\delta} \frac{\left[\left(\pi - 4\sqrt{1-\eta^2}\right)(1-\eta) - 2\eta\sqrt{1-\eta^2} - 2\arcsin\eta + \pi\eta\right]^2}{(1-\eta)^3} d\eta. \qquad (2.38)$$

Integration in Eqs. (2.35) and (2.38) can be performed numerically for any value of ς_b with no difficulty. Then, the right hand side of Eq. (2.28) becomes a function of this parameter. This function should be minimized with respect to ς_b to find the best upper bound based on the kinematically admissible velocity field chosen. This minimization has been carried out numerically assuming that $\delta = 10^{-4}$. Note that the value of ς_b found from this calculation along with f_u is also important because of the restriction $0 < \varsigma_b \le 1$. It has been found that the latter is not satisfied for $h > 0.54$. The variation of f_u with h determined from Eq. (2.28) after minimization is shown in Fig. 2.4 by the broken line. The solid line

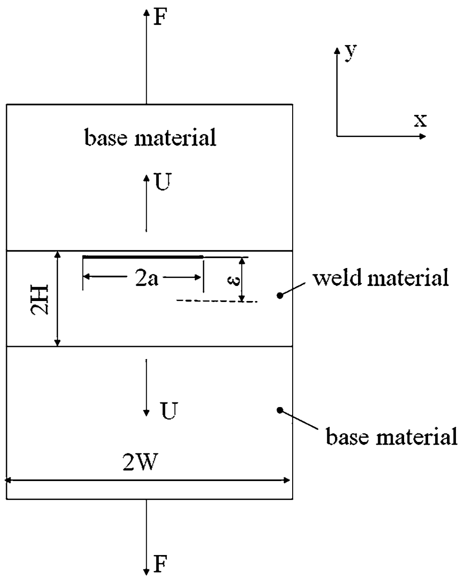

Fig. 2.5 Geometry of the specimen under consideration–notation

corresponds to the solution given by Eq. (2.5). It is seen from this figure that the limit load found from Eq. (2.28) is just slightly higher than that from the accurate numerical solution. An advantage of the solution (2.28) is that a kinematically admissible velocity field similar to that used to arrive at this solution can be constructed for many other structures with no difficulty whereas numerical solutions are usually time-consuming. Moreover, the slip-line technique used to obtain the solution (2.5) is not applicable to non-planar flow of the material obeying the Mises yield criterion. Nevertheless, since the solution (2.5) is available for the problem under consideration, it will be used in subsequent sections. The solution based on the kinematically admissible velocity field (2.9) and (2.11) has been given to show the main difficulties with using singular kinematically admissible velocity fields for finding the limit load and to demonstrate its accuracy by making comparison with the numerical solution.

2.2 Crack at Some Distance From the Mid-Plane of the Weld

The geometry of the specimen and the direction of the axes of Cartesian coordinates (x, y) are illustrated in Fig. 2.5. The only difference from the previous boundary value problem is that a crack is located at some distance ε from the mid-plane of the weld. Its orientation is orthogonal to the line of action of tensile forces F. It is obvious that the sense of ε is immaterial. Therefore, it is possible to assume that $0 \le \varepsilon \le H$. The origin of the coordinate system is located at the intersection of the axes of symmetry of the specimen with no crack. The specimen is symmetric

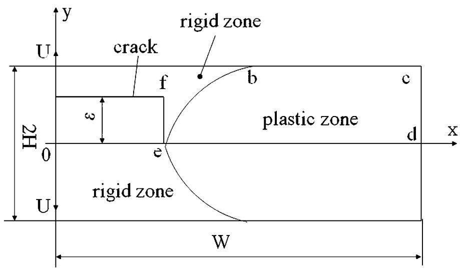

Fig. 2.6 General structure of the kinematically admissible velocity field

relative to the y-axis. Therefore, it is sufficient to find the solution in the domain $x \geq 0$. The center cracked specimen considered in the previous section is obtained at $\varepsilon = 0$. In the case of the interface crack $\varepsilon = H$. A numerical solution for the latter case has been given in Kim and Schwalbe (2001b) where a possible effect of the location of the crack on the limit load is briefly discussed as well.

The general structure of the kinematically admissible velocity field chosen is illustrated in Fig. 2.6 (one half of the weld is shown). The plastic zone is symmetric relative to the x-axis. Therefore, it is sufficient to consider its upper part *ebcd*. The rigid zones move along with the blocks of rigid base material along the y-axis in the opposite directions. The magnitude of velocity of each zone is U. The velocity discontinuity line *ef* separates the two rigid zones. In the plastic zone *ebcd*, the kinematically admissible velocity field can be assumed in the same form as in the zone 0*bdc* shown in Fig. 2.2 (the presence of rigid zone 2 is not essential since any rigid zone can be considered as a special case of plastic zones in which $\zeta_{eq} = 0$.) Then, according to Eq. (2.7) the rate of work dissipation in the plastic zone *ebcd* (Fig. 2.3), including the rate of work dissipation at the velocity discontinuity curves *eb* and *bc* as well as any velocity discontinuity curves inside this zone, is given by

$$E_{ebcd} = \frac{UBW\sigma_0}{\sqrt{3}}\left(1 - \frac{a}{W}\right)\left(3 + \frac{W-a}{H}\right). \tag{2.39}$$

The amount of velocity jump across the velocity discontinuity line *ef* is equal to $|[u_\tau]|_{ef} = 2U$. The area of the corresponding velocity discontinuity surface is $2B\varepsilon$. Therefore, the rate of work dissipation at the velocity discontinuity line *ef* can be found as

$$E_{ef} = \frac{\sigma_0}{\sqrt{3}}\iint\limits_{S_d} |[u_\tau]|_{ef} dS = \frac{2U\sigma_0}{\sqrt{3}}\iint\limits_{S_d} dS = \frac{4UB\varepsilon\sigma_0}{\sqrt{3}}. \tag{2.40}$$

The rate at which external forces F do work is (two equal forces act and one half of the specimen is considered)

$$\iint\limits_{S_v} (t_i v_i) dS = FU. \tag{2.41}$$

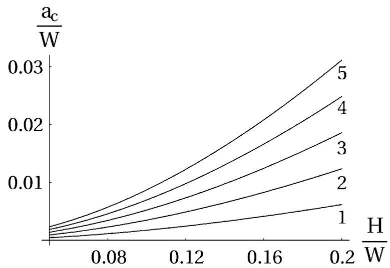

Fig. 2.7 Variation of the critical crack length with H/W at different values of ε

The rate of work dissipation in one half of the specimen is given by $2E_{ebcd} + E_{ef}$. Therefore, it follows from Eqs. (1.4), (2.39), (2.40), and (2.41) that the upper bound limit load is

$$f_u = \frac{F_u}{4BW\sigma_0} = \frac{1}{2\sqrt{3}}\left(1 - \frac{a}{W}\right)\left(3 + \frac{W-a}{H}\right) + \frac{\varepsilon}{W\sqrt{3}}. \tag{2.42}$$

The validity of this solution is restricted by the inequality given after Eq. (2.7). When this inequality is not satisfied (i.e. in the case of large cracks), the solution is trivial and is available in the literature (see, for example, Kotousov and Jaffar 2006). The contribution of the last term in Eq. (2.42) can be too large for small cracks. The kinematically velocity field which has led to the solution (2.5) is also kinematically admissible for the specimen under consideration. Equating $F_u^{(0)}$ from Eq. (2.5) and F_u from Eq. (2.42) gives the following equation for the critical value of $a = a_c$

$$\left(3 + \frac{W}{H}\right) = \left(1 - \frac{a_c}{W}\right)\left(3 + \frac{W-a_c}{H}\right) + \frac{2\varepsilon}{W}. \tag{2.43}$$

The solution to this quadratic equation is trivial and it is illustrated in Fig. 2.7. In this figure, curve 1 corresponds to $\varepsilon/H = 0.2$, curve 2 to $\varepsilon/H = 0.4$, curve 3 to $\varepsilon/H = 0.6$, curve 4 to $\varepsilon/H = 0.8$, and curve 5 to $\varepsilon/H = 1$ (interface crack). In order to determine the best limit load based on the kinematically admissible velocity field chosen, Eq. (2.42) should be used for $a \geq a_c$ and Eq. (2.5) for $a \leq a_c$.

2.3 Arbitrary Crack in the Weld

The geometry of the specimen and Cartesian coordinates (x, y) are shown in Fig. 2.8. The origin of the coordinate system is located at the intersection of the axes of symmetry of the specimen with no crack. In contrast to the specimens considered in the previous sections, the crack may have an arbitrary shape, though some minimal restrictions apply. In particular, it is assumed that the crack is entirely located within the weld and the shape of the crack does not prevent the motion of rigid blocks of material below and above the crack in the opposite

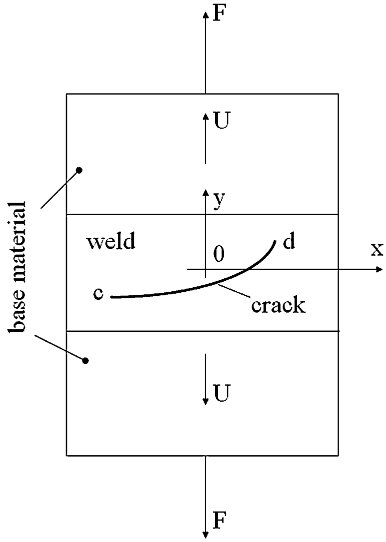

Fig. 2.8 Geometry of the specimen under consideration–notation

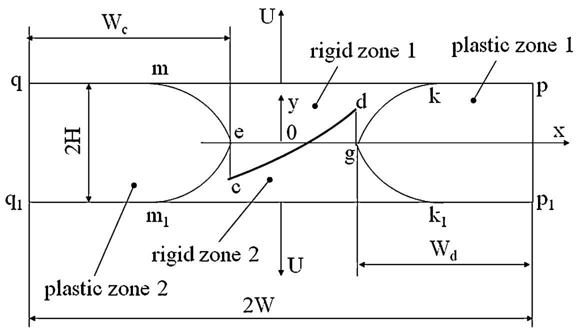

Fig. 2.9 Structure of the kinematically admissible velocity field

directions along the y-axis. An upper bound solution for the specimen under consideration has been proposed in Alexandrov (2010).

The crack is specified by the coordinates of its tips. In particular, $x = x_c$ and $y = y_c$ for tip c, and $x = x_d$ and $y = y_d$ for tip d (Fig. 2.8). By assumption, $x_d \geq 0$ and $x_c \leq 0$. The general structure of the kinematically admissible velocity field chosen is shown in Fig. 2.9. It consists of two plastic zones and two rigid zones. Rigid zone 1 whose boundary is *mecdgk* moves along with the block of rigid base material located above the weld along the positive direction of the y-axis with a velocity U. Rigid zone 2 whose boundary is m_1ecdgk_1 moves along with the block of rigid base material located under the weld along the negative direction of the y-axis with the same velocity. The plastic zones are separated from the rigid zones by the velocity discontinuity curves me, m_1e, kg, and k_1g. Also, there are four velocity discontinuity lines at the bi-material interfaces. Those are qm, q_1m_1, kp, and k_1p_1. Moreover, there are two velocity discontinuity lines separating the rigid zones. Those are ec and dg. Each of the plastic zones is symmetric relative to the x-axis. Therefore, it is sufficient to consider the upper half of each zone. In particular, the kinematically admissible velocity field in the upper half of the plastic zone $pkgk_1p_1$ can be chosen in the same form as in the zone $0bcd$ shown in Fig. 2.2 (the presence of rigid zone 2 is not essential since any rigid zone can be considered as a special case of plastic zones in which $\zeta_{eq} = 0$). Then, according to Eq. (2.5) the rate of work dissipation in the plastic zone $pkgk_1p_1$, including the rate of work dissipation at the velocity discontinuity curves gk and kp as well as at any velocity discontinuity curves inside this zone, is equal to

$$E_{pkgk_1p_1} = \frac{UBW_d\sigma_0}{\sqrt{3}}\left(3 + \frac{W_d}{H}\right). \tag{2.44}$$

It is seen from Fig. 2.9 that $W_d = W - x_d$. Therefore, Eq. (2.44) becomes

$$E_{pkgk_1p_1} = \frac{UB(W - x_d)\sigma_0}{\sqrt{3}}\left(3 + \frac{W - x_d}{H}\right). \tag{2.45}$$

Analogously, for the upper part of the plastic zone $qmem_1q_1$ the rate of work dissipation, including the rate of work dissipation at the velocity discontinuity curves em and mq as well as at any velocity discontinuity curves inside this zone, can be obtained in the following form

$$E_{qmem_1q_1} = \frac{UB(W + x_c)\sigma_0}{\sqrt{3}}\left(3 + \frac{W + x_c}{H}\right). \tag{2.46}$$

It is worth recalling here that $x_c \le 0$. The amount of velocity jump across the velocity discontinuity lines df and ec is $|[u_\tau]|_{df} = |[u_\tau]|_{ec} = 2U$. Therefore, the rates of work dissipation at these lines are

$$E_{df} = \frac{\sigma_0}{\sqrt{3}}\iint\limits_{S_d} |[u_\tau]|_{df} dS = \frac{4UB|y_d|\sigma_0}{\sqrt{3}}, \quad E_{ec} = \frac{\sigma_0}{\sqrt{3}}\iint\limits_{S_d} |[u_\tau]|_{ec} dS = \frac{4UB|y_c|\sigma_0}{\sqrt{3}}. \tag{2.47}$$

The rate at which one external force F does work is given by Eq. (2.41). The rate of total internal work dissipation is $2E_{pkgk_1p_1} + 2E_{qmem_1q_1} + E_{df} + E_{ec}$. Since two identical forces act, it follows from Eqs. (1.4), (2.41), (2.45), (2.46), and (2.47) that

$$\frac{F_u}{4BW\sigma_0} = \frac{(W - x_d)}{4\sqrt{3}W}\left(3 + \frac{W - x_d}{H}\right) + \frac{(W + x_c)}{4\sqrt{3}W}\left(3 + \frac{W + x_c}{H}\right) + \frac{|y_d| + |y_c|}{2\sqrt{3}W}. \tag{2.48}$$

As before, the smallest value between F_u and $F_u^{(0)}$ from Eqs. (2.48) and (2.5), respectively, should be chosen. The solution (2.5) provides a better prediction for small cracks. The solution (2.48) is not valid for large cracks. The restrictions follow from the inequality given after Eq. (2.5) and can be written in the form

$(W - x_d)/H \geq 1$ and $(W + x_c)/H \geq 1$. The solution given in Kotousov and Jaffar (2006) can be adopted when one of these inequalities is not satisfied.

References

S. Alexandrov, A limit load solution for a highly weld strength undermatched tensile panel with an arbitrary crack. Eng. Fract. Mech. **77**, 3368–3371 (2010)

S. Alexandrov, O. Richmond, On estimating the tensile strength of an adhesive plastic layer of arbitrary simply connected contour. Int. J. Solids Struct. **37**, 669–686 (2000)

S. Hao, A. Cornec, K.-H. Schwalbe, Plastic stress-strain fields of a plane strain cracked tensile panel with a mismatched welded joint. Int. J. Solids Struct. **34**, 297–326 (1997)

R. Hill, *The Mathematical Theory of Plasticity* (Clarendon Press, Oxford, 1950)

Y.-J. Kim, K.-H. Schwalbe, Mismatch effect on plastic yield loads in idealised weldments I. Weld centre cracks. Eng. Fract. Mech. **68**, 163–182 (2001a)

Y.-J. Kim, K.-H. Schwalbe, Mismatch effect on plastic yield loads in idealised weldments II. Heat affected zone cracks. Eng. Fract. Mech. **68**, 183–199 (2001b)

A. Kotousov, M.F.M. Jaffar, Collapse load for a crack in a plate with a mismatched welded joint. Eng. Fail. Anal. **13**, 1065–1075 (2006)

L. Prandtl, Anwendungsbeispiele Zu Einem Henckyschen Satz Uber Das Plastische Gleichgewicht. Zeitschr. Angew. Math. Mech. **3**, 401–406 (1923)